Supporting Information

Formation of Morphologically Confined Nanospace via Self-assembly of Graphene and Nanospheres for Selective Separation of Lithium

Yan Zhao,[a] Chen Zhou,[b] Jiaqian Wang,[c] Huawen Liu,[c] Yanqing Xu,[c] Jin Won Seo,[b] Jiangnan Shen,[c,*] Congjie Gao, [c] Bart Van der Bruggen[a,d,*]

[a]Department of Chemical Engineering, KU Leuven, Celestijnenlaan 200F, B-3001 Leuven, Belgium

[b]Department of Materials Engineering, KU Leuven, Kasteelpark Arenberg 44 box 2450, B-3001 Leuven, Belgium

[c]Center for Membrane Separation and Water Science & Technology, Ocean College, Zhejiang University of Technology, Hangzhou 310014, P. R. China

[d]Faculty of Engineering and the Built Environment, Tshwane University of Technology, Private Bag X680, Pretoria 0001, South Africa

*Corresponding author.

Corresponding Authors: shenjn@zjut.edu.cn (Jiangnan Shen)

bart.vanderbruggen@kuleuven.be (Bart Van der Bruggen)

This PDF file includes:

CONTENTS

1. Theories

1.1. Graphene lattice.[1-5]

The six-membered carbon ring of graphene is shown in Fig. S1a. Each of the neighboring carbon atoms provide the dispersion relation of the π electrons near the two Dirac points, which are the in-equivalent points k and k', and is described by the tight-binding model incorporating only the first nearest neighbor interactions

$$E^{\pm}(k_x,k_y) = \pm t\sqrt{1+4cos\frac{\sqrt{3}k_x a}{2}cos\frac{k_y a}{2}+4cos^2\frac{k_y a}{2}} \quad \text{(S1)}$$

$$a = \sqrt{3}a_{CC} \quad \text{(S2)}$$

where, a_{CC} is the distance of each of the neighboring carbon atoms. In theory, the length of a side is 1.42 Å. T is the matrix element between the π orbitals of neighboring carbon atoms. Thus, the maximum diameter of the six-membered carbon ring is 2.84 Å. According to the report, in the experiment, the maximum diameter of the six-membered carbon ring has been estimated around 2.42 Å, which is smaller than any of the metal ions. According to the Hamiltonian of a bilayer graphene near the K-point (inequivalent points in the Brillouin zone), the distance of a bilayer graphene can be calculated and the value is 3.40 Å.

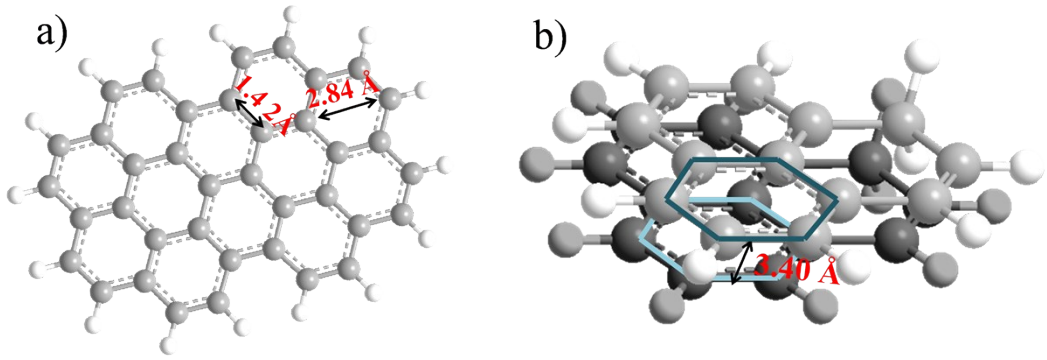

Fig. S1 a) Top of a graphene nanosheet; b) Side view of a bilayer graphene nanosheets.

1.2. The tunable interlayer spacing of multilayer graphene.[3, 4, 6-9]

The 2D structure and the tunable nanoscale interlayer of graphene nanosheets offer an exciting opportunity to make a fundamentally new class of sieving membranes. In the multilayer structure of graphene membrane, hydrated ions permeate through the interconnected nanochannels formed between graphene nanosheets and follow a tortuous path primarily over the hydro-phobic nonoxidized surface. The interlayer size of dry graphene oxide (GO) membrane is about 3 Å. However, when the wet GO membrane was immersed in water, the hydrated reaction increased the GO spacing to 9 Å. Thus, only ions with a hydrated diameter of 9 Å or less could enter the nanochannel. In this case, controlling the tunable nanoscale interlayer of graphene nanosheets is the most important thing. For example, the small nano-particles or functional materials used to limit the size of interlayer. As shown in Fig. S2a and S2b, the small spacing could be obtained with small-sized molecules in theory.

Due to the flexibility and chemical stability of the GO nanosheet, it is difficult to control the spacing in virture. In addition, without any of the interaction, the particles will easily loss from the multilayer structure in separation process.

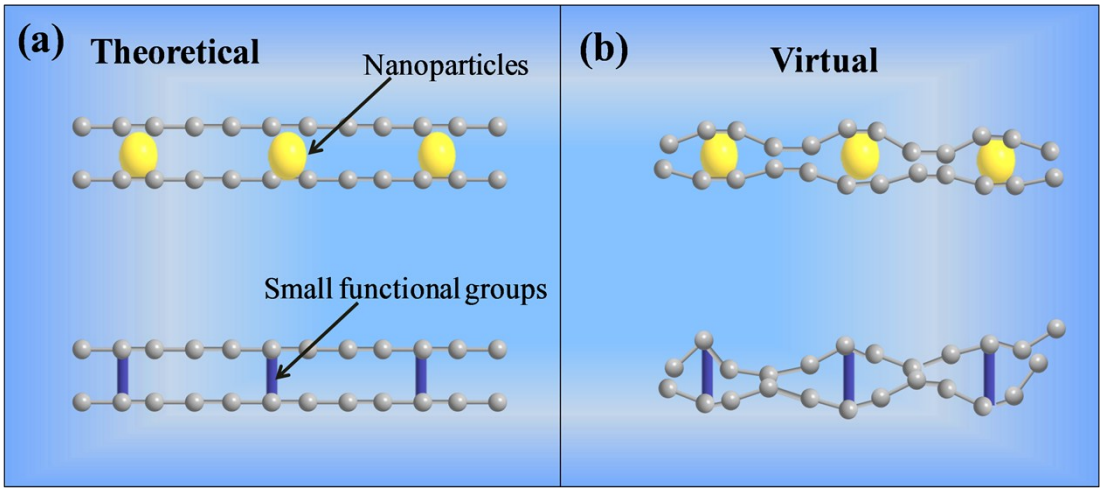

Fig. S2 The theoretical (a) and virtual (b) control the tunable interlayer spacing of multilayer graphene.

1.3. The mechanism of rGO@SAPS membrane for selective separation and ions transport.[10, 11]

The separation of Li^+, K^+ and Mg^{2+} by rGO@SAPS membrane in electrodialysis (ED) was shown in Fig. S3a. In order to analysis the mechanism of rGO@SAPS membrane for selective separation of lithium ion, firstly, the hydrated ion and its energy should be provided.

The around of hydrated Li^+, K^+ and Mg^{2+} could be seen as the Coordination-Solvent mixing Zone and Random change Zone as demonstrated in our previous work. The coordination number of water molecules (C_N), which in the Coordination-Solvent mixing Zone, part of the water molecules forms a coordination bond with the ion, was calculated by

$$C_N = \frac{(r_{M^{Z+}} + r_{H_2O})^3}{r_{M^{Z+}}^3} \quad \text{(S3)}$$

where $r_{M^{Z+}}$ is the radius of cation (metal ions); r_{H_2O} is the radius of water molecular and Z^+ is the valence number of metal ions.

Some water molecules are not forms a coordination bond with the metal ions. Here, we named them as non-coordination water molecule and the non-coordination number of water molecules is also called solvent number of water molecules (S_N).

The totally ionic hydration energy ΔG was calculated by

$$\Delta G = U_c + U_s + U_r + U_h + U_p \quad \text{(S4)}$$

In this process, the U_c is the energy of C_N and calculated by

$$U_c = \frac{N_A \cdot e^2 \cdot Z^2}{\varepsilon \cdot r_{M^{Z+}}} \cdot (C_N) \quad \text{(S5)}$$

U_s is the energy of C_N and was calculated by

$$U_s = 13.2 \cdot \frac{Z^2}{r_{M^{Z+}}^2} \cdot (S_N) \quad \text{(S6)}$$

where e is the quantity of electric charge; ε is the dielectric constant; the N_A is the Avogadro constants.

U_r is the rotational energy of water molecules in coordination-solvent mixing zone.

$$U_r = \frac{n \cdot i}{2RT} \quad \text{(S7)}$$

$$U_r^{'} = \frac{U_r}{n \cdot N_A} \quad \text{(S8)}$$

$$\overline{U_r} = \frac{i}{2KT} \quad \text{(S9)}$$

where n is the molar weight; i is the rotational degrees of freedom of water molecule; R is the thermodynamic parameters; T is the thermodynamic temperature; $U_r^{'}$ is the rotational energy of each water molecule in coordination-solvent mixing zone; $\overline{U_r}$ is the average rotational energy of water molecules in coordination-solvent mixing zone. the Boltzmann constant is

$$K = \frac{R}{N_A} \quad \text{(S10)}$$

U_h is the hydrogen bond energy and each of the hydrogen bond energy is about 18.81kJ·mol^{-1} and the number of hydrogen bond (HBN) in the Coordination-Solvent mixing Zone could be calculated by

$$HBN = (C_N) - Z \quad \text{(S11)}$$

U_p is the Polarization energy of water molecules, which in the random change zone and was calculated by

$$U_p = \frac{\alpha \cdot (Z^*)^2}{r_{M^{Z+}}} \quad \text{(S12)}$$

where Z* is the effective relative permittivity. α is a constant and related to the electronic configurations.

As show in Fig. S3b and S3c, the hydrated Li^+, K^+ and Mg^{2+} cross the rGO@SAPS need to overcome the above ionic hydration energy in electrodialysis (ED) process. Besides, lower binding affinity results led to the difficult condensation of the cation-sulfonate pairs, and thus the easier cations transportation, as shown in Fig. S3d.

The transport mechanism is the ion sieving effect between the rGO@SAPS membrane structure and cations hydrated ionic diameter, and mobility of cations. Here, we provided the Mg^{2+}, K^+ and Li^+ hydrated ionic diameter, as shown in Table 1. Due to the mechanism of its hydrated ion and its energy, the size of Mg^{2+} hydrate (0.86 nm) is larger than that of Li^+ and K^+, which means the Mg^{2+} more difficult through the membrane than Li^+ and K^+.

In this work, the cyclic voltammetry curves are typically used to show the capacitance behavior of the membrane, which suggests the membrane capacity of adsorption and desorption of ions. As shown in Fig. 3f, the ion-exchange capacitance cyclic voltammetry curves is 0.35 (Mg^{2+}), 0.22 (K^+) and 0.03 (Li^+), respectively. The results were closer to their corresponding binding affinity to sulfonate groups (normalized to Li^+), which is 1.0 (Li^+), 2.90 (K^+) and 3.18 (Mg^{2+}), respectively. Lower binding affinity results led to a difficult condensation of the cation-sulfonate pairs, and thus an easier cation transport. Thus, Li^+ can pass through the rGO@SAPS-2 membrane easier than other cations, which suggests that our membrane could be useful in Li^+ extraction.

Therefore, the size sieving effect and the binding affinity contribute to the rGO@SAPS membranes with the selective separation of Li^+.

Table 1. Hydrated radius of cations.

Cation species	Li^+	K^+	Mg^{2+}

Hydrated radius (nm)	0.764	0.662	0.856

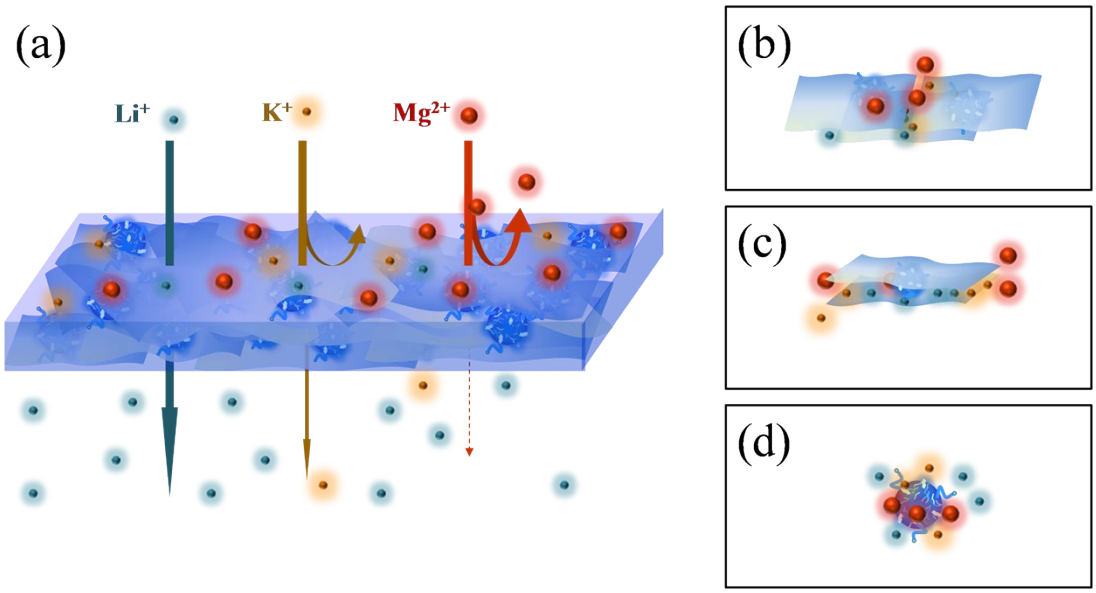

Fig. S3 The mechanism of rGO@SAPS membrane for selective separation of lithium ion (a); hydrated Li^+, K^+ and Mg^{2+} cross the aperture of two rGO nanosheets (b) and interlayer of the rGO@SAPS (c) process.

1.4 The selectivity efficiency.[12-15]

The separation efficiency parameter was provided by Van der Bruggen et al., which used to evaluate the selective separation between two kinds of ions. The separation efficiency S between component A and B,

$$S(t) = \frac{((c_A(t))/(c_A\,(0)\,)) - ((c_B\,(t))/(c_B\,(0)\,))}{(1-(c_A(t))/(c_A(0)\,)) + (1-((c_B(t))/(c_B(0)\,))} \times 100\% \qquad \text{(S13)}$$

where $c_A(0)$ and $c_B(0)$ are the initial concentration of Mg^{2+} (K^+) and Li^+, respectively; and $c_A(t)$ and $c_B(t)$ are the concentration of Mg^{2+} (K^+) and Li^+ at time t.

1.5 The permselectivity.[16-19]

The permselectivity value was applied to evaluate the flux of ions selective separation through the membrane. The permselectivity of the membranes between component A and B, P_A^B was calculated by

$$P_A^B = \frac{t_B/t_A}{c_B/c_A} = \frac{J_B \cdot c_A}{J_B \cdot c_A} \quad \text{(S14)}$$

where t_i (t_A and t_B) is the transport number of the ions through the membrane, J_i (J_A and J_B) is the flux of the ions through the membrane expressed in mol/m^2·s. The t_i was calculated

$$t_i = \frac{J_i z_i F}{I} \quad \text{(S15)}$$

where z_i is the ion charge, F is Faraday's constant and I is the DC current. The flux of ions was obtained from the change in concentration of the ions on the dilute side according to

$$J_i = \frac{V \cdot \frac{dc_i}{dt}}{A} \quad \text{(S16)}$$

where V is the volume of the electrolyte solution in dilute compartment and A is the active area of the membranes.

1.6 The flux of cations.[15, 20, 21]

In order to further evaluate the separation of cations through the rGO@SAPS membranes, the flux of cations, which is the decrease of the concentration of total cations, were provided here and calculated

$$D\ (t) = \sum \left(c_k(0) - c_k(t)\right) \quad \text{(S17)}$$

where D is the decrease of the total cations concentration in dilute compartment and k is the types of cations. c(0) and $c_k(t)$ is the concentration of K in initial and time t, respectively.

2. Materials

Latex beads, amine-modified polystyrene (0.05 μm, 2.5% w/v), Graphite powder (99.95%), potassium permanganate, potassium persulfate ($K_2S_2O_8$), phosphorus pentoxide (P_2O_5), hydrogen peroxide (30%) (H_2O_2), sulfuric acid (98%) (H_2SO_4), hydrochloric acid (HCl) and sodium hydroxide (NaOH) were analytical reagent and obtained from Aladdin Industrial Co., Ltd (Shanghai, China). 1-ethyl-3-(3-dimethylami-nopropyl) carbodiimide hydrochloride (EDC-HCl) and N-hydroxy succinimide (NHS) were purchased from Macklin Biochemical Co., Ltd (Shanghai, China). Lithium chloride (LiCl) were purchased from BDH Laboratory Supplies Poole, BH151TD (England), Magnesium chloride ($MgCl_2$) were purchased from Alfa Aesar GmbH&Co KG (Karlsruhe, Germany), potassium chloride (KCl) were purchased from Industriezone “De Arend” (Belgium), Sodium sulfate (Na_2SO_4) were purchased from New Jersey (USA).

3. Methods

3.1 Synthesis of graphene oxide (GO).

According to the Hummer's method, GO was prepared from graphite powder. 0.625 g of $K_2S_2O_8$, 0.625 g of P_2O_5 and 0.1873 g of natural graphite powder were added into 3.3 mL H_2SO_4 in an ice-water bath, under stirring of 750 rpm. Then the mixture was improved to 80 ℃ in the oil bath. 4.5 hours later, the mixture was washed by pure water until ph=7 and obtained the purification of graphite powder by suction filtration. Then dry the graphite powder by vacuum drying oven. After that, 0.187 g of the dry graphite powder was added to 30 mL of H_2SO_4 of flask under stirring (250 rpm) at ice-water bath. Then, 3.75 g of $KMnO_4$ were added into the flask slowly. Successively, the temperature was improved to 35 ℃ and stirred at 750 rpm. 2 hours later, 62.5 mL of distilled water was added slowly and the temperature was increased very quickly at this time. 1 hours later, an additional 175 mL water was added. Followed, slow addition of 5 mL of H_2O_2 (30%) was added into it and the mixture was filtered and washed with diluted HCl aqueous (1/10 v/v) to remove metal ions. The obtained sample was collected and dried in vacuum freezing drying oven for 48 hours.

3.2 Synthesis of sulfonated amino-polystyrene nanosphere (SAPS).

5 mL amine-modified polystyrene nanospheres (0.05 μm, 2.5% w/v) was dry into the vacuum oven and dispersed into the 50 mL fuming H_2SO_4 by ultrasonic dispersion in the ice-water. 2 hours later, transformed into oil bath in 50 ℃ and stirred at 750 rpm. 12 hours later, the pale white solution would get and cool to room temperature. Then, washed with ethanol and 4 times centrifugation and dispersed into the 50 mL pure water.

3.3 Synthesis of amino-polystyrene nanosphere sulfonate chemical self-assembled multilayer graphene (rGO@SAPS) membrane.

100 mg of GO was dispersed in 120 mL pure water (200 mg/mL) by using ultrasone in 40 KHz. Then, the mixture was kept in the oil bath at 25 °C under stirring at 300 rpm. Then, the SAPS solution (2.5, 5 and 10 mL), which was prepared as shown in step 3.2, was added to the mixture, respectively. At the same time, 100 mg of EDC-HCl and 60 mg of NHS as the catalyst were added into the mixture in 750 rpm. 24 hours later, the samples were washed by pure water for three times and named as and named GO@SAPS-1, GO@SAPS-2 and GO@SAPS-3, respectively. The solution was fabricated by filtering the above flocculent suspension on a Polycarbonate (PC) (PC membrane (Whatman) with pore size of 200 nm, and effective diameters of 19 mm were used for the preparation of the composite paper by vacuum filtration.) support using a SIBATA filtration system and each of the mixture solution could be obtained 3 membranes. After peeling from the PC, the films were dried in 25℃. Finally, the obtained membrane were placed into a 100 mL Teflon-sealed autoclave with 70 mL water and heated to 180 ℃ for 10 h. After that, the films were immersed into 0.01 M NaOH for 24 hours, and then immersed into distilled water three times before drying at 60 ℃ for 12 hours. At last, the rGO@SAPS-1, rGO@SAPS-2 and rGO@SAPS-3 membranes were obtained, respectively.

3.4 Total reflectance Fourier transforms infrared (ATR-FTIR).

The functional groups information was monitored by total reflectance Fourier transform infrared spectroscopy (ATR-FTIR) (Nicolet 6700, The United States) at room temperature. GO@SAPS membranes were dried thoroughly in vacuum oven at 45°C prior to measurements.

3.5 Scanning electronic microscopy (SEM).

The morphologies and structures of GO@SAPS and rGO@SAPS membranes (surface and cross-sectional) were characterized using scanning electronic microscopy (SEM) (Hitachi S-4800) at an accelerating voltage of 15.0 kV. The EDS maps C, O, N and S element over the cross-section were provided at the same time.

3.6 Transmission electron microscopy (TEM).

Projected area and cross-section images of samples were obtained using a probe-lens corrected JEOL ARM200F operating at 200 kV, equipped with cold-field emission source and Centurio energy dispersive X-ray spectroscopy (EDS) detector.

3.7 X-ray diffraction (XRD)

The GO, rGO and as-prepared rGO@SAPS membranes were characterized by X-ray diffraction (XRD) at 0.02 degree step at room temperature using an X'Pert PRO (PANalytical, Netherlands) instrument with Cu Kα radiation.

3.8 X-ray photo-electron spectroscopy (XPS).

The elemental composition of the GO@SAPS and rGO@SAPS membranes were analyzed by X-ray photo-electron spectroscopy (XPS, Kratos AXIS Ultra DLD, Japan). The anode was mono (Al (Mono)) (45 W). The charge neutralizer was on current 1.8 A, balance 3.3 V and bias 1.0 V.

3.9 Electrochemical impedance spectroscopy (EIS) measurement.

Electrochemical impedance spectroscopy (EIS) results were used to evaluated the membranes' electric resistance and obtained from a frequency range of 100 kHz to 1 Hz by an electrochemical workstation (AUTOLAB AUT86804, the Netherlands) in the voltage range 0-3.5 V with a scan rate of 0.1 $mV \cdot S^{-1}$.

3.10 Polarization current-voltage.

The free-standing electrodes were tested to confirm the initial electrochemical performance. The polarization current-voltage curve is an important variable to characterize the performance of electrochemical membranes. As we shown in our previous work, in a wide range of currents, it displays three different regions, which are Ohmic region, plateau region and over limiting region, respectively. The GO, rGO and as-prepared rGO@SAPS membranes were directly used as working electrode without any binder and carbon black. The GO, rGO and the hydrothermal as-prepared rGO@SAPS membranes electrode were prepared and pasted onto pure copper foils, then pressed and dried under vacuum at 60 °C for 12 h. The electrolyte was 1 M Na_2SO_4. The electrochemical performances of the GO, rGO and as-prepared rGO@SAPS membranes were tested by an electrochemical workstation in the voltage range of 0-1.5 V with a scan rate of 0.1 $mV \cdot S^{-1}$.

3.11 Cyclic voltammetry measurement

The cyclic voltammetry curves usually used to show the capacitance behavior of the membrane, which means the membrane capacity of adsorption and desorption of ions. The electrolyte were used1 M LiCl, KCl and $MgCl_2$, respectively. They were tested by an electrochemical workstation in the voltage range of 0-0.6 V with a scan rate of 0.1 $mV \cdot S^{-1}$.

3.12 Selective separation of lithium ion measurement

In this work, 250 mL·min^{-1} of solution velocity, 12.73 mA·cm^{-2} of current density and 10 μm thickness of the membrane was applied to measure the membranes' selective separation. 0.05 M $MgCl_2$, KCl and LiCl mixed solution was applied in both compartments in contact with the membrane. The electrode solution was a 0.2 M Na_2SO_4 solution. In the dilute compartment, the concentration of mixtures of Mg^{2+}, K^+ and Li^+ was measured by inductively coupled plasma (ICP) every 20 min.

4. Results

4.1 The TEM images of GO@SAPS-1 and GO@SAPS-3.

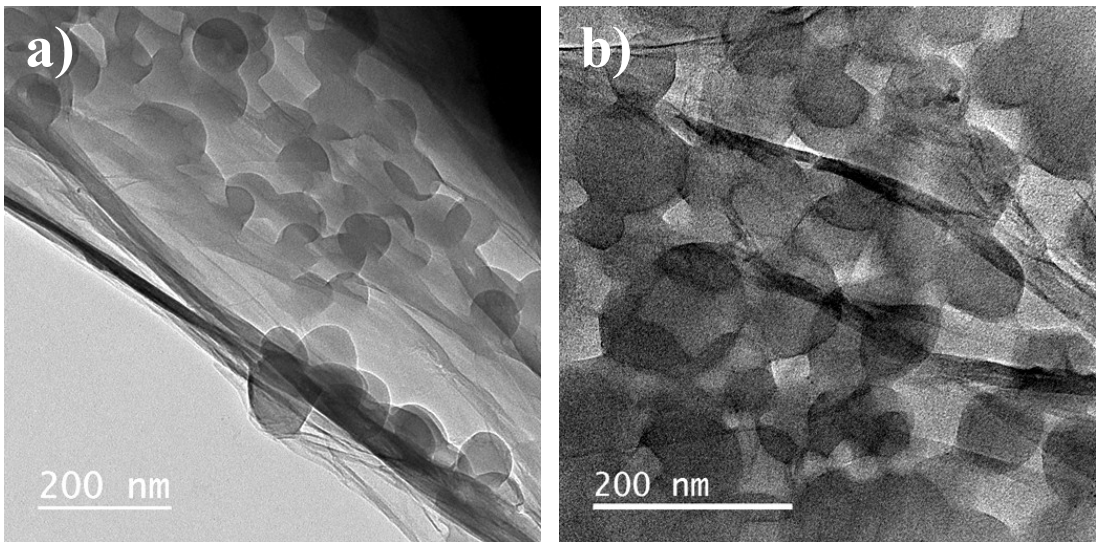

Fig. S4 TEM images of GO@SAPS-1 (a) and GO@SAPS-3 (b).

4.2 The mechanism of selective separation of Li^+.

In this work, the negatively charged rGO@SAPS membranes were used for ion separation in ED process. The electric field force was used as a driving force that lead ions transport the membranes. As shown in Fig. S5, under the electric field force, Mg^{2+}, K^+ and Li^+ transport from one compartment to another through the negatively charged rGO@SAPS membranes. The Mg^{2+}, K^+ and Li^+ transported the rGO@SAPS membranes in an ion-exchange way. Usually, the electrostatic repulsive force between the fixed charges of the membranes' surface and the common-ions in solution, the ions

sieving effect between the membrane structure and hydrated ionic diameter, and mobility of different ions are the mainly basic theory for the ion exchange membranes with the selective separation of ions. In this work, the ion sieving effect between the rGO@SAPS membrane structure and cations hydrated ionic diameter, and mobility of Mg^{2+}, K^+ and Li^+ are the two main mechanism of selective separation of Li^+

Firstly, the negatively charged SAPS were firmly grafted on the surface of GO nanosheets by chemical bond (-NH-OC-). The resulting rGO@SAPS membranes have the morphologically confined nanospace of interlayer between rGO and SAPS. The hydrated diameters of Mg^{2+}, K^+ and Li^+ are 0.86, 0.66 and 0.76 nm, respectively. Besides, according to the mechanism hydrated Li^+, K^+ and Mg^{2+}, the hydrated ion and its energy should be provided. As demonstrated in the mechanism of rGO@SAPS membrane for selective separation, the hydrated Li^+, K^+ and Mg^{2+} cross the rGO@SAPS need to overcome the above ionic hydration energy in electrodialysis (ED) process. The size of Mg^{2+} hydrate (0.86 nm) is larger than that of Li^+ and K^+, which means the Mg^{2+} is more difficult through the membrane than Li^+ and K^+.

Secondly, the mobility of Mg^{2+}, K^+ and Li^+ is $Mg^{2+} < K^+ < Li^+$, due to the mobility affected by their corresponding binding affinity to sulfonate groups. The binding affinity to sulfonate groups (normalized to Li^+) is 1.0 (Li^+), 2.90 (K^+) and 3.18 (Mg^{2+}), respectively. It was also confirmed by the size of ion-exchange capacitance CV curves, which is 0.35 (Mg^{2+}), 0.22 (K^+) and 0.03 (Li^+), respectively. That means the Li^+ much easier through the rGO@SAPS membranes than K^+ and Mg^{2+}.

Therefore, the size sieving effect and the binding affinity contribute to the rGO@SAPS membranes with the selective separation of Li^+.

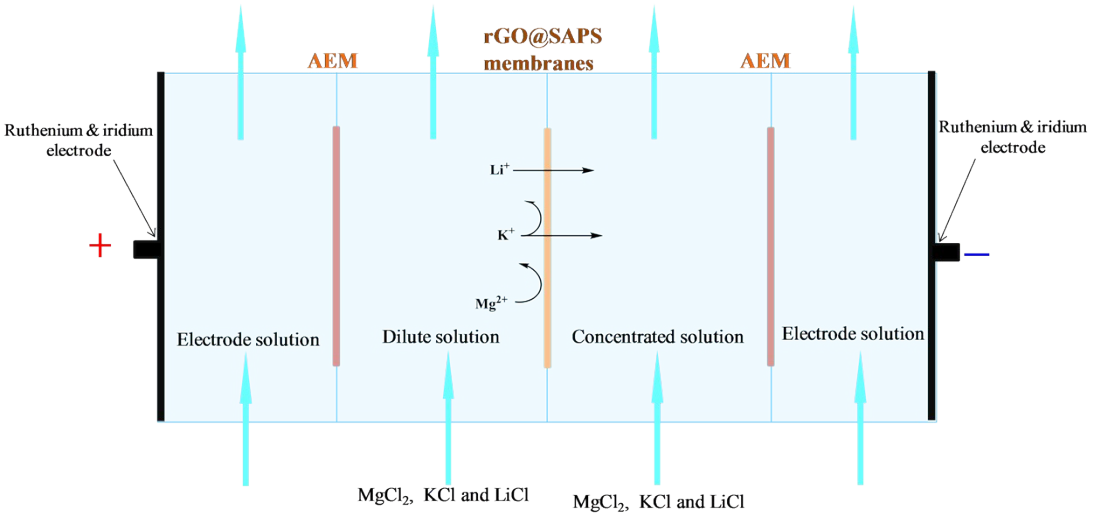

Fig. S5 The mechanism of selective separation of Li^+ in ED.

4.3 TEM image of GO@SAPS-1 and GO@SAPS-3membrane and the EDS elemental maps.

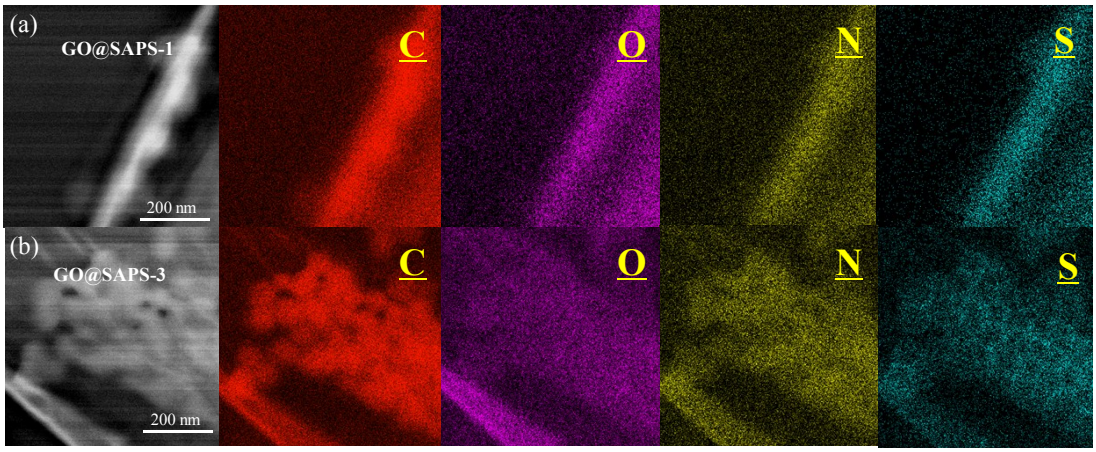

Fig. S6 The GO@SAPS-1 (a) and the GO@SAPS-3 (a) membranes' TEM element mapping images

4.4 X-ray photoelectron spectroscopy (XPS) was used to detect surface elements for GO@SAPS and rGO@SAPS membranes.

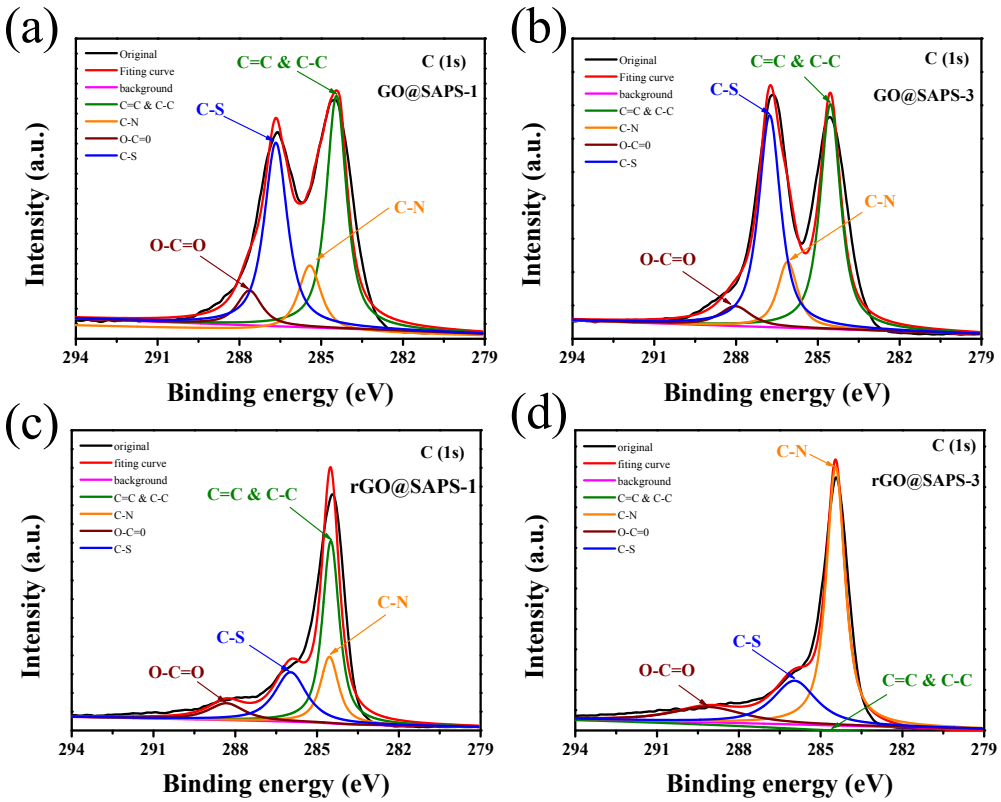

Fig. S7 XPS images of GO@SAPS-1 (a), GO@SAPS-3 (b), rGO@SAPS-1 (c) and rGO@SAPS-3 (d) membranes.

4.5 The surface elements (atomic %) of resulting membranes.

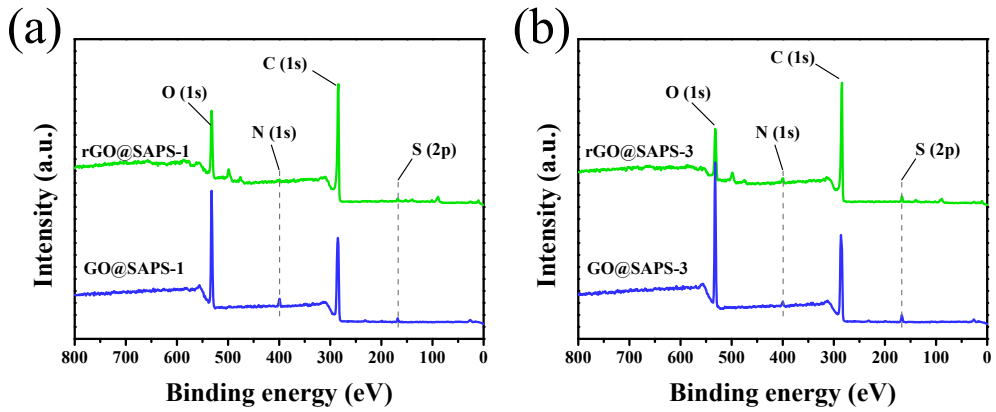

Fig. S8 XPS images of surface elements (atomic %) of GO@SAPS-1 and rGO@SAPS-1 (a); GO@SAPS-3 and rGO@SAPS-3 (b).

Table 2. The surface elements of different resulting membranes.

Membrane Types	Atomic %			
	O 1s	N 1s	C 1s	S 2p
GO@SAPS-1	27.26	3.72	67.95	1.07
GO@SAPS-2	29.9	2.05	66.91	1.14
GO@SAPS-3	30.07	1.95	66.78	1.2
rGO@SAPS-1	19.07	1.61	77.07	2.24
rGO@SAPS-2	16.15	2.25	79.17	2.43
rGO@SAPS-3	14.25	2.17	81.3	2.28

4.6 The lab-made electrodialysis device for selective separation of lithium.

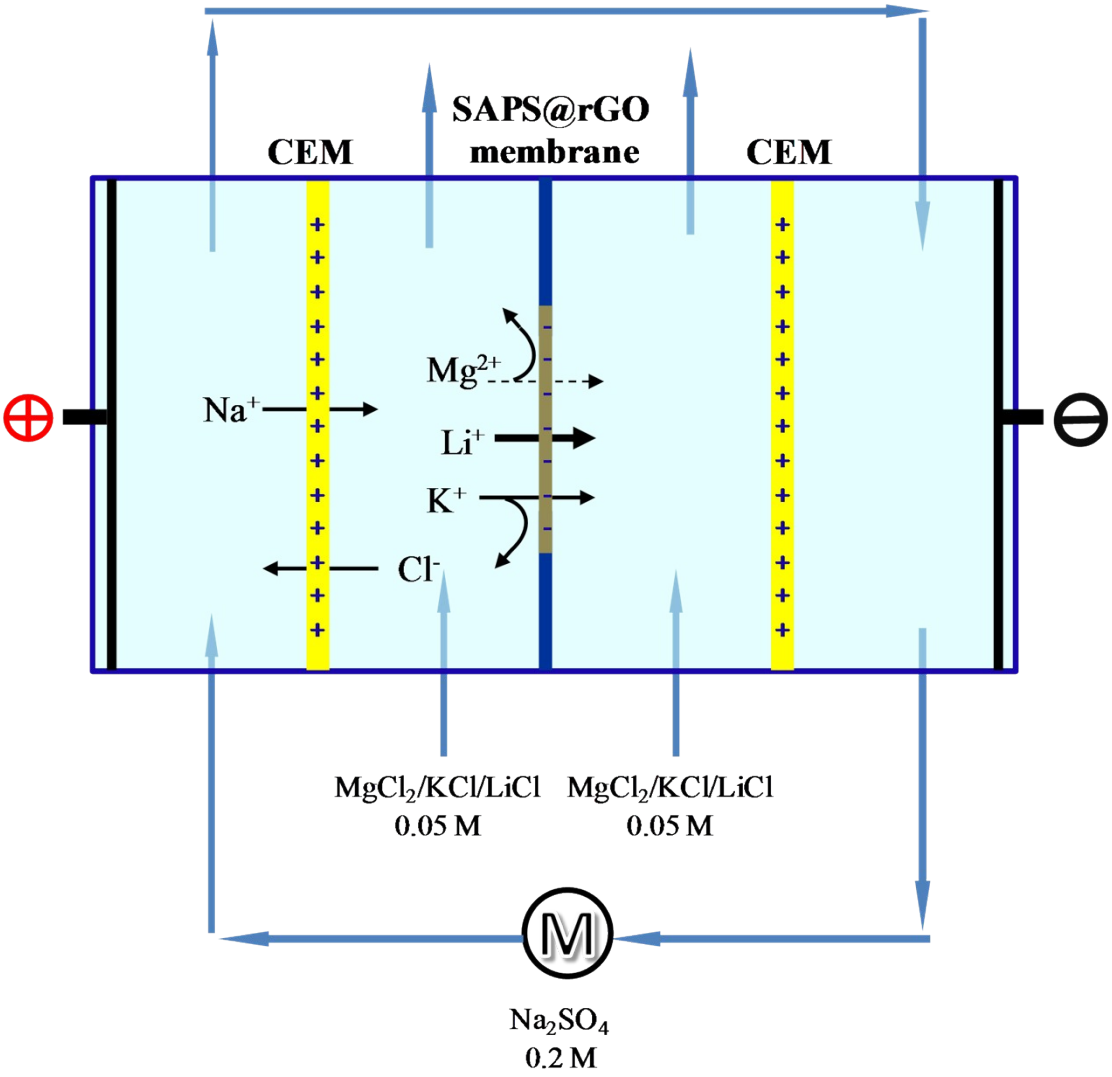

Fig. S9 The scheme of lab-made electrodialysis device for selective separation of lithium ion.

4.7 The process of selective separation of lithium.

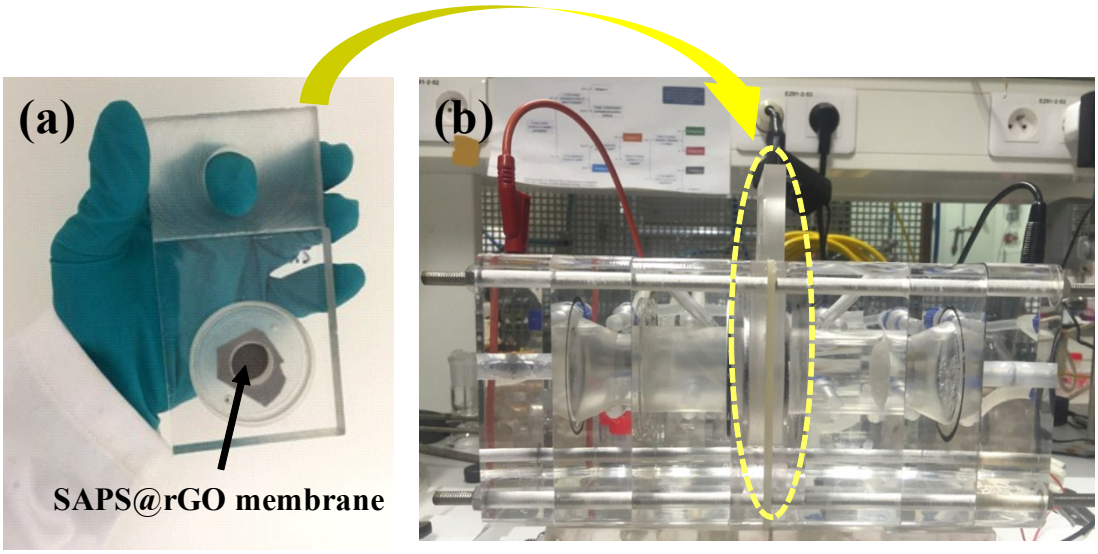

Fig. S10 The rGO@SAPS-1, rGO@SAPS-2 and rGO@SAPS-3 membranes were fixed into the device respectively (a) and the device of ions separation process.

4.8 The concentration of Li^+, K^+ and Mg^{2+} in the dilute compartment.

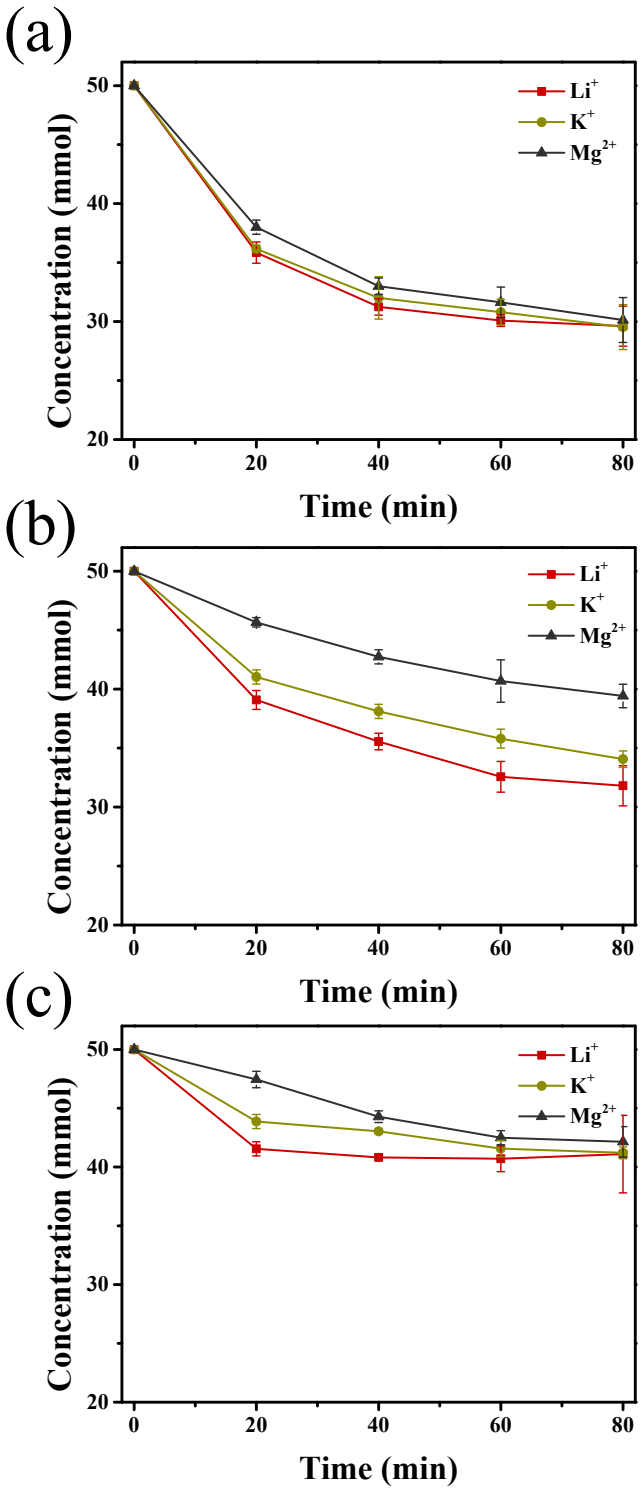

Fig. S11 In the dilute compartment, the concentration of Li^+, K^+ and Mg^{2+} in ED process through rGO@SAPS-1, rGO@SAPS-2 and rGO@SAPS-3, respectively, were measured by the inductively coupled plasma mass spectrometry (ICP-MS) every 20 min.

5. References

1. C. N. Rao, A. K. Sood, K. S. Subrahmanyam, A. Govindaraj, *Angew. Chem. Int. Edit*, 2009, **48**, 7752-7777.
2. Y. Zhu, S. Murali, W. Cai, X. Li, J. W. Suk, J. R. Potts, R. S. Ruoff, *Adv. Mater.*, 2010, **22**, 3906-3924.
3. B. Mi, *Science*, 2014, **343**, 740-742.
4. D. Chen, L. Tang, J. Li, *Chem. Soc. Rev.*, 2010, **39**, 3157-3180.
5. V. Singh, D. Joung, L. Zhai, S. Das, S. I. Khondaker, S. Seal, *Prog. Mater. Sci.*, 2011, **56**, 1178-1271.
6. X. Huang, X. Qi, F. Boey, H. Zhang, *Chem. Soc. Rev.*, 2012, **41**, 666-686.
7. D. Li, M. B. Muller, S. Gilje, R. B. Kaner, G. G. Wallace, *Nat. Nanotechnol.*, 2008, **3**, 101-105.
8. Y. Li, H. Wang, L. Xie, Y. Liang, G. Hong, H. Dai, *J. Am. Chem. Soc.*, 2011, **133**, 7296-7299.
9. Q. Xiang, J. Yu, M. Jaroniec, *J. Am. Chem. Soc.*, 2012, **134**, 6575-6578.
10. Y. Zhao, W. Shi, B. V. der Bruggen, C. Gao, J. Shen, *Adv. Mater. Interfaces*, 2018, **5**, 1701449.
11. Y. Zhao, J. Zhu, J. Li, Z. Zhao, S. I. C. Ochoa, J. Shen, C. Gao, B. V. der Bruggen, *ACS Appl. Mater. Interfaces*, 2018, **10**, 18426-18433.
12. Y. Zhao, K. Tang, H. Ruan, L. Xue, B. Van der Bruggen, C. Gao, J. Shen, *J. Membrane Sci.*, 2017, **536**, 167-175.
13. Y. Zhao, K. Tang, Q. Liu, B. Van der Bruggen, A. S. Díaz, J. Pan, C. Gao, J. Shen, *RSC Adv.*, 2016, **6**, 16548-16554.
14. N. White, M. Misovich, A. Yaroshchuk, M. L. Bruening, *ACS Appl. Mater. Interfaces*, 2015, **7**, 6620-6628.
15. K. W. Song, C. K. Kim, *J. Membrane Sci.*, 2010, **352**, 239-246.
16. F. Z. Pengzhan Sun, Miao Zhu, Zhigong Song, Kunlin Wang, Minlin Zhong, Dehai Wu, Reginald B. Little, Zhiping Xu, and Hongwei Zhu, *ACS NANO*, **8**,

850-859.

17. E. Güler, W. van Baak, M. Saakes, K. Nijmeijer, *J. Membrane Sci.*, 2014, **455**, 254-270.
18. S. Mulyati, R. Takagi, A. Fujii, Y. Ohmukai, H. Matsuyama, *J. Membrane Sci.*, 2013, **431**, 113-120.
19. J. W. Post, H. V. M. Hamelers, C. J. N. Buisman, *J. Membrane Sci.*, 2009, **330**, 65-72.
20. L. Yu, Y. Zhang, B. Zhang, J. Liu, H. Zhang, C. Song, *J. Membrane Sci.*, 2013, **447**, 452-462.
21. Y. Ruan, Y. Zhu, Y. Zhang, Q. Gao, X. Lu, L. Lu, *Langmuir*, 2016, **32**, 13778-13786.